Biol. Cybern. 75, 1–9 (1996)

Biological Cybernetics

A random walk model of fast-phase timing during optokinetic nystagmus

Thomas J. Anastasio

Beckman Institute and Department of Molecular and Integrative Physiology, University of Illinois at Urbana/Champaign, Urbana, IL 61801, USA

Received: 1 June 1995/Accepted in revised form: 15 February 1996

Abstract. Most vertebrate animals produce optokinetic nystagmus in response to rotation of their visual surround. Nystagmus consists of an alternation of slow-phase eye rotations, which follow the surround, and fast-phase eye rotations, which quickly reset eye position. The time intervals between fast phases vary stochastically, even during optokinetic nystagmus produced by constant velocity rotation of a uniform surround. The inter-fast-phase interval distribution has a long tail, and intervals that are long relative to the mode become even more likely as constant surround velocity is decreased. This paper provides insight into fast-phase timing by showing that the process of fast-phase generation during constant velocity optokinetic nystagmus is analogous to a random walk with drift toward a threshold. Neurophysiologically, the output of vestibular nucleus neurons, which drive the slow phase, would approximate a random walk with drift because they integrate the noisy, constant surround velocity signal they receive from the visual system. Burst neurons, which fire a burst to drive the fast phase and reset the slow phase, are brought to threshold by the vestibular nucleus neurons. Such a nystagmic process produces stochastically varying inter-fast-phase intervals, and long intervals emerge naturally because, as drift rate (related to surround velocity) decreases, it becomes more likely that any random walk can meander for a long time before it crosses the threshold. The theoretical probability density function of the first threshold crossing times of random walks with drift is known to be that of an inverse Gaussian distribution. This probability density function describes well the distributions of the intervals between fast phases that were either determined experimentally, or simulated using a neurophysiologically plausible neural network model of fast-phase generation, during constant velocity optokinetic nystagmus.

Correspondence to: T. J. Anastasio, University of Illinois, Beckman Institute, 405 North Mathews Ave., Urbana, IL 61801, USA

1 Introduction

In most vertebrate animals, visual images are stabilized on the retinae during movement in space by the concerted actions of the vestibular and optokinetic systems (Robinson 1989). This active stabilization occurs during translational and rotational movements in three dimensions, but it has been studied mainly for rotation in the horizontal plane because that type of motion is the most easily produced in the laboratory. The vestibulo-ocular system produces rotations of the eyes that oppose rotations of the head, by feeding input forward from the semicircular canal receptors which essentially transduce head rotational acceleration. The optokinetic system uses visual feedback to match the rotational velocity of the eyes with the perceived rotational velocity of the visual surround as the animal rotates its head within the environment. The vestibular and optokinetic systems produce relatively slow eye rotations that serve to stabilize the retinal image during movement, and these slow rotations are interrupted periodically by fast eye rotations that quickly reset eye position. The alternation of slow-phase and fast-phase eye rotations constitutes vestibular and optokinetic nystagmus.

A central problem in the study of nystagmus is the timing of fast phases. Most previous models concerned vestibular nystagmus (Schmid and Lardini 1976; Chun and Robinson 1978; Galiana 1991). These models attempted to reproduce the nystagmic pattern that resulted from transient or sinusoidal head rotational acceleration stimuli. Because the timing of fast phases is stochastic, the nystagmic pattern resulting from time varying stimulation is complex and difficult to quantify (Chun and Robinson 1978). Unfortunately, the long-duration rotational accelerations that would provide a constant vestibular stimulus are difficult to produce. The optokinetic system offers an advantage in the study of nystagmus in that constant stimulation can be easily produced using constant velocity surround rotation. Large numbers of fast phases at the same constant level of nystagmus can be generated, and this facilitates the analysis of fast-phase timing.

Constant velocity surround rotation was used recently by Balaban and Ariel (1992) to study the intervals

between fast phases generated during optokinetic nystagmus in the turtle. They found that the inter-fast-phase interval (IFPI) distribution had a long tail, and that IFPIs that were long relative to the mode became even more likely as the velocity of the constant surround rotation decreased. They modeled the data using a timing mechanism which generated a fast phase at some random but predetermined time following the previous fast phase, and long IFPIs occurred when, under certain circumstances, the interval timing mechanism skipped a cycle.

The purpose of this paper is to propose an alternative model of fast-phase timing during constant surround velocity optokinetic nystagmus. It is based on the neurophysiology of the oculomotor system (Robinson 1975, 1989). Eye position commands, which drive the slow phase, are generated by vestibular nucleus neurons which integrate the velocity signals they receive. Fast-phase commands are generated by burst neurons, which are brought to threshold by vestibular nucleus neurons. Importantly, the constant surround velocity signal provided by the visual system is noisy (Collewijn 1975; Hoffmann and Schoppmann 1981; Hoffmann and Distler 1989). Therefore, after this signal is integrated by the vestibular nucleus neurons it should approximate a random walk (integrated noise) with drift (integrated constant), and it is this signal that should bring the burst neurons to threshold. This scheme generates long IFPIs naturally because, as drift rate (related to surround velocity) decreases, it becomes more likely that any random walk can meander for a long time before it crosses the threshold.

The neurophysiological process for fast-phase generation sketched out above is analogous to a random walk with drift toward a threshold. A random walk with drift (Wiener diffusion process) is defined as a random process $X(t)$ that at any time $t > 0$ has a Gaussian distribution with mean vt and variance $\sigma^2 t$, where $v > 0$ and $\sigma^2 > 0$ are referred to as the drift rate and diffusion constant, respectively. To determine the theoretical distribution of the first threshold crossing times for random walks with drift, the equation $X(t) = \alpha$, where α is the threshold value, is solved for t such that $X(u) < \alpha$ for all $u < t$. The distribution of the solution is known (Seshadri 1993) to be an inverse Gaussian distribution whose probability density function (pdf) is:

$$f(t) = \frac{\tilde{\alpha}}{\sqrt{2\pi}} t^{-3/2} \exp\left\{ -\frac{(\tilde{\alpha} - \tilde{v}t)^2}{2t} \right\}, \quad t > 0 \qquad (1)$$

where $\tilde{v} = v/\sigma$ and $\tilde{\alpha} = \alpha/\sigma$. The parameters $\tilde{v}$ and $\tilde{\alpha}$ will be referred to simply as drift rate and threshold, respectively, and they are the free parameters to be determined in fitting equation (1) to empirical IFPI distributions. The fitting procedure essentially treats IFPI data as random samples from the inverse Gaussian distribution. This is equivalent to making the simplifying assumption that successive IFPIs are independent. The diffusion constant (σ^2), which can be thought of loosely as the noisiness of the process, is assumed not to vary over experimental conditions.

The inverse Gaussian pdf (1) describes well the distributions of IFPIs that were generated during constant velocity optokinetic experiments in goldfish (and turtle, Balaban and Ariel 1992), or simulated using a neurophysiologically plausible neural network model of fast-phase command generation. The concordance of the theory with both the experimental and computational results supports the idea that fast-phase generation during constant velocity optokinetic nystagmus is analogous to a random walk with drift toward a threshold.

2 Methods

Experiments were conducted on two comet goldfish (*Carassius auratus*), about 16 cm in length. The fish were tested during their normal waking hours. Each fish was wrapped in gauze and restrained in an experimental tank using contoured body supports. Its mouth was opened over a plastic tube and secured to it with a loop of string. The fish was artificially respired with fresh water from a reservoir that was pumped through the tube. A small coil of Teflon-insulated copper wire (20 turns, 5.3 mm external coil diameter) was attached to the left eye, concentric with the pupil, using two loops of ophthalmic suture (6–0 monofilament). The experimental tank had a key-hole-shaped layout. The head of the fish was centered within the cylindrical front end, which was made of clear Plexiglas, and permitted an unobstructed view of the surroundings, through the water and tank, of 280 deg horizontally and 80 deg vertically.

The experimental tank was placed within an apparatus equipped with magnetic field generating coils and an eye coil preamplifier. An optokinetic drum was suspended around the tank inside the field coils. The drum had alternating black and white stripes that subtended 7.8 and 8.9 deg, respectively. The drum was illuminated from above using four 60 W lamps. The drum was rotated around the fish at constant rotational velocity using a servo-controlled motor. The drum tachometer signal was calibrated during constant velocity rotations by measuring the time intervals between synch pulses that occurred once per revolution. Drum rotation elicited optokinetic nystagmus from the fish, which consisted of alternating slow and fast phases.

Eye rotational position was transduced using the magnetic search-coil technique (Robinson 1963; Remmel 1984). After each experiment, the eye coil was detached from the eye, repositioned in the magnetic field at the same place, and calibrated with a protractor. A high-pass filter was used to differentiate the eye position signal, which converted the fast phases into sharp eye velocity spikes which were then window discriminated and converted into uniform pulses. The eye position and drum tachometer signals were antialias filtered (8-pole Butterworth, 25 Hz cut-off frequency) and digitized (12 bit A/D, 50 Hz sampling rate) using a computer interface (1401, Cambridge Electronic Design). The interface simultaneously time stamped fast-phase and drum synch pulses to resolutions of 1 and 10 ms, respectively. Analog/digital conversion and pulse timing were thus separate but

synchronized processes occurring at different temporal resolutions. Data acquisition began only after the optokinetic response had reached steady state.

Data analysis and modeling were performed in the MATLAB programming environment (The MathWorks). Eye velocity was computed by digitally differentiating eye position. Fast-phase occurrence time data were checked with an interactive routine. Two types of triggering errors could occur: either a pulse could be triggered in the absence of a fast phase (spurious trigger), or a fast-phase velocity spike could fail to reach the threshold for a pulse (drop-out). The checking routine first removed spurious triggers by removing all fast-phase occurrence times that had IFPIs of less than a preset tolerance (100 ms). It then displayed eye velocity together with the remaining pulses and allowed any drop-outs or other missing pulses to be inserted. The temporal resolution of the inserted pulses was limited to that of the eye velocity data (20 ms), but inserted pulses accounted for less than 2% of all fast-phase pulses. The routine continued to cycle through the data set until an entire pass without any insertions was made. This ensured that the fast-phase occurrence time data were free of triggering errors.

Fast-phase command generation was simulated using a neural network model. The dynamics of the model were discrete in time. The model simulates the activity of brainstem neurons during optokinetic nystagmus, in which a fast-phase command consists primarily of a burst in the activity of a neural element representing burst neurons. Simulated bursts were detected and timed using an automatic threshold algorithm, and the burst occurrence times were verified using the same checking routine that was used for real fast phases as described above.

The time intervals between goldfish fast phases, or simulated fast-phase commands, were computed and IFPI histograms were constructed. The bin width for each IFPI histogram was equal to the mean IFPI divided by 15. In addition, a histogram of turtle optokinetic IFPIs was taken from the literature (Balaban and Ariel 1992). In all cases, the proportion density of the IFPIs was computed from the histogram by dividing the proportion of IFPIs in each bin by the bin width, so that the total area of the IFPI proportion density distribution was equal to 1. The inverse Gaussian pdf (1) was fit to the IFPI proportion density distributions by standard least squares, but the error measure is reported as:

$$P_{\text{err}} = \frac{1}{2}\Delta\sqrt{\sum_{i=1}^{n}(d_i^{\text{the}} - d_i^{\text{emp}})^2} \tag{2}$$

where d_i^{the} and d_i^{emp} are the theoretical and empirical densities, respectively, Δ is the bin width, n is the number of bins, and P_{err} is referred to as the probability error. It is related to the total squared error, which is the expression under the radical, and the smaller it is the better the fit. However, P_{err} is more readily interpretable as it roughly approximates the measure:

$$P^*_{\text{err}} = \frac{1}{2}\Delta\sum_{i=1}^{n}|d_i^{\text{the}} - d_i^{\text{emp}}| \tag{3}$$

The geometric interpretation of P^*_{err} is one half of the area between the two density functions, theoretical and empirical. The measure P^*_{err} is bounded between 0 (perfect fit) and 1 (when the two pdfs do not overlap at all), and it can be interpreted as a probability measure (an inverse analogue of a conventional p value). The measure P_{err} is easier to minimize, however, as this only requires standard least squares. Because the sampling distributions of P_{err} and P^*_{err} are not known, conventional p values for goodness-of-fit cannot be reported. Conventional measures, however, would not be useful. Because the random walk with drift analogy is meant here as a reasonable approximation rather than a precise null hypothesis, the inability to reject it would only indicate a lack of sufficient sample sizes to do so.

3 Results

The results comprise fits of the inverse Gaussian pdf to IFPI distributions that were either generated during optokinetic experiments, taken from the literature, or simulated.

3.1 Experimental results

Optokinetic nystagmus was elicited in two goldfish by rotating a visual surround (uniformly striped drum) around them at constant velocity. Previous work has demonstrated that the optokinetic response in goldfish is robust between about 3 and 40 deg/s constant velocity surround rotation, and that it is asymmetrical, being stronger for surround rotation in the temporal to nasal direction (Easter 1972). The two fish were tested with surround rotations of 6, 12 and 30 deg/s in the preferred (temporal to nasal) direction. A segment of the eye rotational position record during optokinetic nystagmus for 12 deg/s surround rotation in goldfish 1 is shown in Fig. 1A. Positive eye positions are in the nasal direction. The optokinetic response had the typical nystagmic pattern, and consisted of slow phases that follow the rotation of the surround and fast phases that quickly rotate the eye in the opposite direction. As previously reported in goldfish (Easter 1972), the range of eye positions is smaller during optokinetic nystagmus than it is for spontaneous eye rotations (not shown).

The eye position data were digitally differentiated and the resulting eye rotational velocity trace is shown in Fig. 1B. The fast phases appear as sharp spikes in eye velocity of up to 200 deg/s in the direction opposite to that of surround rotation (temporal, negative). The slow phase appears as a constant eye velocity of almost 10 deg/s in the direction of surround rotation (nasal, positive). Slow-phase eye velocity is taken as a measure of the magnitude of the optokinetic response in goldfish and the values are listed in Table 1A and B. The magnitude of the optokinetic response roughly doubled in going from surround rotations of 6 to 12 deg/s but, because the optokinetic response saturates in goldfish (Easter 1972), it only roughly doubled again in going from 12 to 30 deg/s.

The fast-phase data were reduced by constructing histograms of the time intervals between them. The IFPI histogram for the fast phases that occurred during optokinetic nystagmus elicited by surround rotation of 12 deg/s in goldfish 1 is shown in Fig. 2A. (A sample of the nystagmus from which these IFPIs were taken is shown in Fig. 1.) The fast-phase data were further reduced by computing the proportion density of the IFPIs from the IFPI histogram. The proportion density gives an estimate of the probability density of the IFPIs. The IFPI proportion density distribution data were fit with the inverse Gaussian pdf (1). The IFPI proportion density distribution that was computed from the IFPI histogram of Fig. 2A, and the fit of (1) to this IFPI proportion density distribution, are shown in Fig. 2B (circles and curve, respectively).

The IFPI data in Fig. 2 appear symmetrically distributed. However, the shape of the IFPI distributions varied with the velocity of the surround rotation that was used to elicit optokinetic nystagmus, and also varied between individual goldfish at the same surround velocities. IFPI

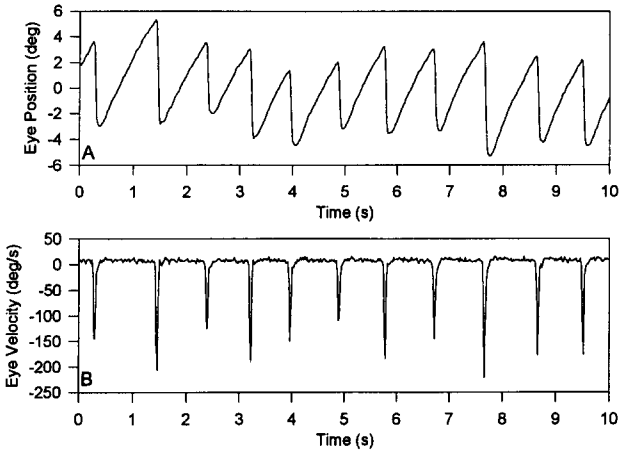

Fig. 1A, B. Horizontal optokinetic nystagmus in a goldfish. The eye rotational position (**A**) of goldfish 1 was digitized during constant velocity surround rotation at 12 deg/s in the preferred (temporal to nasal) direction. The response shows the typical nystagmic pattern of alternating slow and fast phases. Eye rotational velocity (**B**) was computed from position by digital differentiation. Fast phases appear as velocity peaks up to 200 deg/s in amplitude. Positive eye positions and velocities are in the nasal direction

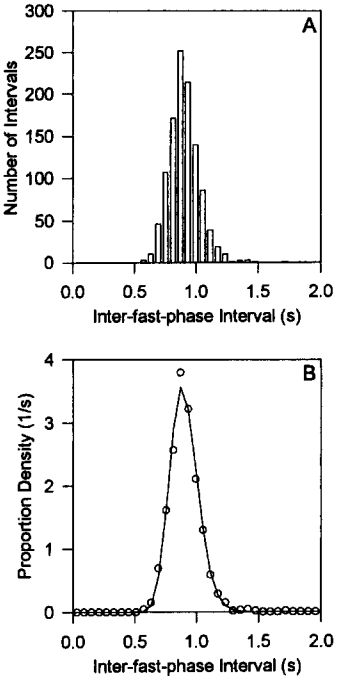

Fig. 2A, B. Distribution of inter-fast-phase intervals (IFPIs) during horizontal optokinetic nystagmus in a goldfish. The nystagmus was elicited from goldfish 1 during constant velocity surround rotation at 12 deg/s in the preferred direction; a sample of this response is shown in Fig. 1. The histogram (**A**) shows the numbers of IFPIs falling within 0.060 s bins; the total number of intervals is 1105. The IFPI proportion density distribution (**B**, *circles*) was computed from the IFPI histogram and fit with the inverse Gaussian probability density function (**B**, *curve*). The best fit parameters are given in Table 1A

Table 1. Parameters for real inter-fast-phase interval (IFPI) proportion density distributions and for fits to the distributions of the inverse Gaussian probability density function (1)

Drum velocity (deg/s)	Eye velocity (deg/s)	Drift rate (σ units)	Threshold (σ units)	Probability error	Bin width (s)	No. of bins	No. of intervals
A. HOKN fast-phase data of goldfish 1							
6	5.307	4.833	5.675	0.017	0.078	39	415
12	8.278	8.355	7.550	0.014	0.060	50	1105
30	19.465	12.183	6.889	0.016	0.038	80	1761
B. HOKN fast-phase data of goldfish 2							
6	5.359	3.578	6.464	0.027	0.120	25	276
12	8.786	5.060	6.118	0.034	0.078	39	828
30	18.200	8.081	5.384	0.021	0.044	68	1465
C. HOKN fast-phase data in turtle (Balaban and Ariel 1992)							
21	Unknown	0.784	2.676	0.029	0.455	33	468

Data were obtained during horizontal optokinetic nystagmus (HOKN) elicited by constant velocity surround (drum) rotation in the horizontal plane. Eye velocity is a measure of optokinetic response magnitude, which is presumed to be related to the input to the fast-phase generator. The drift rate and threshold are in σ units (see Introduction). The probability error value is calculated according to (2)

proportion density distributions for surround rotations of 6, 12 and 30 deg/s (squares, circles and triangles, respectively) are shown for goldfish 1 and 2 in Fig. 3A and B, respectively. The average IFPI increases as surround velocity decreases. Also, the distributions become broader and more skewed toward long intervals as surround velocity decreases. The IFPI distributions are broader for goldfish 2 than for goldfish 1 at each surround velocity.

The inverse Gaussian pdf [(1), curves in Fig. 3] provides an adequate description of the data at all surround velocities in both goldfish. Parameters for the fits are given in Table 1A and B. Drift rate estimates clearly increase as slow-phase eye velocity increases, indicating that optokinetic response magnitude is related to drift rate in the random walk analogy. Threshold estimates show no consistent trend and hover around an average of about 6 in both fish, suggesting that threshold was minimally affected by the changes in surround velocity. The drift rate and threshold estimates are of roughly the same order of magnitude.

An IFPI histogram for fast phases generated during optokinetic nystagmus at a surround velocity of 21 deg/s in the turtle was taken from the literature (Balaban and Ariel 1992), converted into proportion density, and replotted in Fig. 4 (circles). This asymmetrical, long-tailed distribution differs from the goldfish distributions in that the IFPIs are about 5 times longer, even though the surround velocity of 21 deg/s is in the same range as that used in the goldfish experiments (6–30 deg/s). The turtle IFPI proportion density distribution is also adequately described by the inverse Gaussian pdf [(1), curve in Fig. 4]. Parameters for the fit are given in Table 1C. The drift rate and threshold estimates are lower for the turtle than for the goldfish. Also, drift rate is roughly an order of magnitude lower than threshold in the turtle, whereas these estimates are of roughly the same order of magnitude in the goldfish.

3.2 *Computational model*

A simplified model of optokinetic nystagmus was constructed to demonstrate that the neurophysiological considerations that lead to the random walk with drift analogy can be realized by a plausible neural network. The commands to eye muscle motoneurons that drive optokinetic and vestibular nystagmus are generated by a network of premotor neurons that include vestibular nucleus neurons and burst neurons (Shimazu 1983). Basically, the vestibular nucleus neurons and burst neurons generate, respectively, motor commands for the slow and fast phases of nystagmus. The proper coordination of these neurons during nystagmus may involve pause neurons, the continuous activity of which is interrupted only during fast eye movements (Keller 1974). The model, which is schematized in Fig. 5, consists of single neural elements that represent populations of bias (BS), optokinetic input (IN), vestibular nucleus (VN), burst (BN) and pause (PN) neurons. Excitatory and inhibitory connections are represented by arrows and circles, respectively, and the numbers near the connections indicate the values of the arbitrarily assigned weights. All the connection weights have absolute value 1, except for the inhibitory connections to BN (see below). The firing rates of the neurons simply represent the weighted sums of their inputs, and would be linear except that they have a lower bound at 0. The architecture of the network

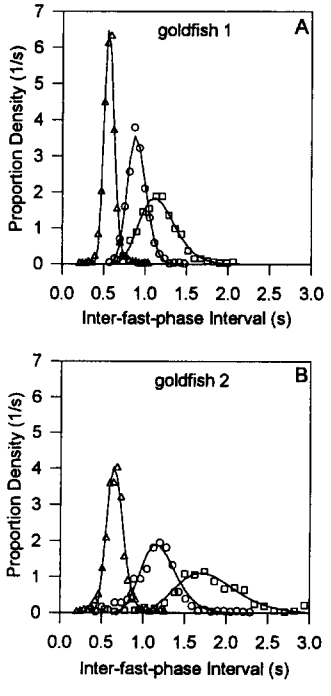

Fig. 3A, B. Fitting the inverse Gaussian probability density function (pdf) to inter-fast-phase interval (IFPI) distributions in goldfish. The proportion densities of the IFPIs during horizontal optokinetic nystagmus were determined for constant velocity surround rotations of 6, 12 and 30 deg/s (*squares*, *circles* and *triangles*, respectively) in goldfish 1 (**A**) and goldfish 2 (**B**). The IFPI proportion density distribution for drum rotation of 12 deg/s in goldfish 1 is reproduced from Fig. 2. The IFPI proportion density distributions were fit with the inverse Gaussian pdf (*curves*). The best fit parameters are given in Table 1A and B

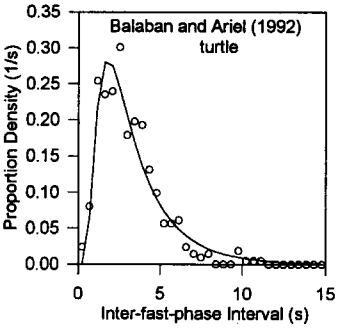

Fig. 4. Fitting the inverse Gaussian probability density function (pdf) to an inter-fast-phase interval (IFPI) distribution in turtle. The IFPI histogram for horizontal optokinetic nystagmus during constant drum rotation of 21 deg/s was determined in a turtle. The histogram data were taken from Fig. 2B of Balaban and Ariel (1992). The IFPI proportion density distribution (*circles*) was computed from the IFPI histogram and fit with the inverse Gaussian pdf (*curve*). The best fit parameters are given in Table 1C

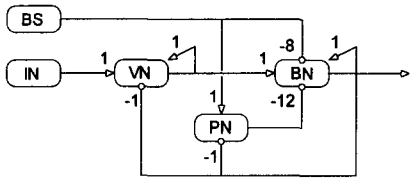

Fig. 5. A neural, integrate-to-fire model of fast-phase generation in the optokinetic system. Excitatory and inhibitory connections are shown as *arrows* and *circles*, respectively. The *numbers* indicate the connection weights. *BS*, bias; *IN*, input; *VN*, vestibular nucleus neuron; *BN*, burst neuron; *PN*, pause neuron

is based upon neuroanatomical and neurophysiological findings.

Vestibular nucleus neurons respond to optokinetic stimulation (Waespe and Henn 1977; Boyle et al. 1985). Optokinetic input is supplied to the vestibular nuclei by neurons in the nucleus of the optic tract in the pretectum (Watanabe et al. 1993). Neurons in the nucleus of the optic tract have an irregular (i.e., noisy) response to optokinetic stimulation (Collewijn 1975; Hoffmann and Schoppmann 1981; Hoffmann and Distler 1989). Neuron IN provides an optokinetic input to VN in the model (Fig. 5).

The optokinetic input encodes the velocity with which the image of the visual surround sweeps across the retina, and this velocity signal must be integrated to produce a position command that is needed to drive the eyes during the slow phases of nystagmus (Robinson 1975, 1989). It has been suggested that this neural integration is brought about by positive feedback in the vestibular nuclei. Vestibular nucleus neurons on one side of the brainstem inhibit their counterparts on the opposite side through inhibitory interneurons (Shimazu and Precht 1966; Nakao et al. 1982). This reciprocal inhibition could result in net positive feedback, which in turn could mediate the process of neural integration (Cannon et al. 1983; Galiana and Outerbridge 1984). Neural integration in the vestibular nucleus is represented in the model by positive feedback of VN onto itself (Fig. 5).

Pause neurons strongly inhibit burst neurons (Keller 1974; Nakao et al. 1980). Burst neurons form two groups that make either excitatory or inhibitory connections with other neurons (Shimazu 1983). Inhibitory burst neurons project to pause neurons (Langer and Kaneko 1984). Excitatory burst neurons may also inhibit pause neurons (Strassman et al. 1986a, b), and can inhibit vestibular nucleus neurons (Sasaki and Shimazu 1981), through inhibitory interneurons. Excitatory burst neurons may excite themselves through relays in the reticular formation (Strassman et al. 1986a, b). Additionally, excitatory burst neurons excite inhibitory burst neurons (Sasaki and Shimazu 1981; Strassman et al. 1986a, b). Therefore, since the excitatory and inhibitory burst neurons are functionally coupled (Galiana 1991), the two types are combined into a single burst neuron element (BN) that can make both excitatory and inhibitory connections. Finally, burst neurons can be driven by vestibular nucleus neurons either directly (McCrea et al. 1987) or through relay neurons found in the nucleus prepositus and adjacent reticular formation (Ohki et al. 1988). These connections, simplified by removing interneurons and relay neurons, are represented in the model (Fig. 5).

The experimental findings described above are from mammals, primarily cats and monkeys. Because goldfish produce an optokinetic nystagmus pattern very similar to that observed in mammals (Easter 1972), and because vestibular nucleus neurons in goldfish respond to optokinetic stimulation (Allum et al. 1976), it is assumed that the functional circuitry described above for mammals is applicable to goldfish also. A bias element (BS) is explicitly represented in the model, which provides a constant input to BN and PN (Fig. 5). This bias to burst and pause neurons could represent nonspecific inputs from other neurons or, equivalently, could result from the biophysical properties of the neurons themselves.

3.3 Computational results

The model (Fig. 5) was used to simulate fast-phase generation during optokinetic nystagmus in the goldfish. It functions essentially as an integrate-to-fire mechanism. The integrating element is VN. It integrates the constant optokinetic input supplied to it by IN, and sends the results of its integration to BN. The firing element is BN. BN is inhibited by BS, which has a constant rate of 1. BS also provides a background rate of 1 for PN, which in turn also inhibits BN. The total inhibition of BN is -20 (-8 from BS and -12 from PN), and this is the threshold of the integrate-to-fire mechanism. When the integrated input from VN to BN exceeds this threshold, the total input to BN becomes positive and BN starts to fire. This closes the positive feedback loop from BN onto itself, causing BN to rapidly increase its firing rate. BN inhibits PN, thereby disinhibiting itself, and this causes the firing rate of BN to increase even more rapidly. The high firing rate of BN at this point is enough to switch off VN, even though the rate of VN has built up to a high level. Without its excitatory drive from VN, the rate of BN quickly falls due to inhibition of BN by BS, and then by PN, after the now rapidly decreasing rate of BN releases PN from inhibition. The inhibition of BN switches it off, and VN is able to begin integrating its input again. The process, having gone full cycle, is repeated.

The model generates fast phases at a rate that depends upon its connection weights, and upon the magnitude of the optokinetic input (IN). In the absence of noise, the model will generate fast phases with uniform IFPIs, as the output of VN drifts up at a uniform rate to the threshold of BN and is reset. A larger input increases VN drift rate, and this results in shorter IFPIs. Adding noise to the model will cause the IFPIs to vary stochastically. Noise was introduced into the model by adding a random number from a Gaussian distribution to the input of an element at each time step. Gaussian noise was chosen on the assumption that input to a real neuron represents the sum of a large number of converging parallel channels. Each input channel is stochastic and, although the noise distribution for each one cannot be specified, the distribution of noise from the combined channels will

approximate a Gaussian distribution by the central limit theorem of statistics. The effect of the noise in the model depended upon its variance, and upon the identity of the element to which it was added. For example, adding noise to BN effectively added jitter to the threshold. This produced IFPIs (not shown) that were symmetrically distributed about the mean, with a relatively small variance that depended upon the variance of the noise. Although the mean IFPI increased as input (IN) magnitude decreased, the shape of the IFPI distribution was not affected by the magnitude of the input. Therefore, noise at the BN level cannot alone account for the IFPI data, where distribution shape clearly depends on input magnitude (Fig. 3).

Noise added to VN is integrated, and this integrated noise approximates a random walk. When noise is added along with the constant optokinetic input from IN, the output of VN approximates a random walk with drift. An example is shown in Fig. 6A of the output of VN with added noise, input magnitude 0.50, and model time step set at 20 ms (the temporal resolution of the goldfish optokinetic data). The noise had a Gaussian distribution with mean 0 and variance 0.50. The random walk component causes a meandering in the drift of the VN output up to the threshold of BN, and this produces variability in the intervals between the bursts, as shown in Fig. 6B. Due to the delay in the network, the output of VN continues to increase above the BN threshold (threshold = 20) for a part of the burst duration before BN begins to shut VN off. With the connection weights chosen (Fig. 5), the BN burst height is about 50% larger than the VN output at its peak, which agrees well with experimental results from vestibular nucleus and burst neurons during nystagmus (Hikosaka et al. 1977). The noisy ramp output of VN in the model is also in good qualitative agreement with that observed for real vestibular nucleus, nucleus prepositus, and adjacent reticular formation neurons during nystagmus (Hikosaka et al. 1977, 1978; Curthoys et al. 1981; Nakao et al. 1982).

The model (Fig. 5) was used to simulate fast-phase command generation during optokinetic nystagmus, with Gaussian noise (mean 0 and variance 0.50) and various magnitudes of constant input to VN. The proportion density distribution of the simulated IFPIs was calculated, and is shown in Fig. 7 for inputs to VN with magnitudes of 0.25, 0.50 and 1.00 (squares, circles and triangles, respectively). (A sample of simulated fast-phase generation at input magnitude 0.50 is shown in Fig. 6.) The progressive doubling of the input magnitudes was intended to match the approximate doubling of the magnitudes of the responses of the goldfish optokinetic system in going from surround rotations of 6 to 12 deg/s, and from 12 to 30 deg/s (see above). The Gaussian noise variance of 0.50 was chosen to achieve a better qualitative match between the simulated and real data. (Gaussian noise with mean 0 and variance 1 produced simulated IFPI distributions with a variance qualitatively larger than that of the data.) The inverse Gaussian pdf [(1), curves in Fig. 7] provides a good description of the simulated data at all input magnitudes. Parameters for the fits are given in Table 2. Probability errors for simulated and real data are comparable.

The simulated (Fig. 7) and real (Fig. 3) data are in good qualitative agreement, and an even closer match to any particular experimentally determined IFPI proportion density distribution could be achieved by adjusting input magnitude and noise variance in the model. For both the simulated and real data, the IFPI distribution becomes narrower and less skewed toward long IFPIs as input magnitude increases. This is reflected in the parameter values (Tables 1A and B, 2), where drift rate increases as input magnitude increases. The threshold estimate for the simulated data is about 6 on average, as for the real data.

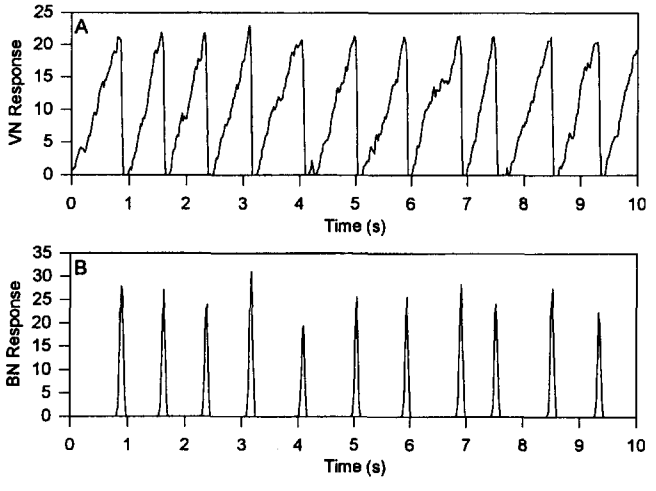

Fig. 6A, B. Operation of the neural, integrate-to-fire model of fast-phase generation in the optokinetic system. The vestibular nucleus neuron (VN in Fig. 5) receives random noise (Gaussian distributed with mean 0 and variance 0.50) and a constant input of 0.50, and its integrated output approximates a random walk with drift (**A**). The vestibular nucleus neuron response was fed to the burst neuron (BN in Fig. 5) which fired a burst (**B**) whenever its excitatory input exceeded its inhibitory input. The inhibitory input to the burst neuron is analogous to the threshold

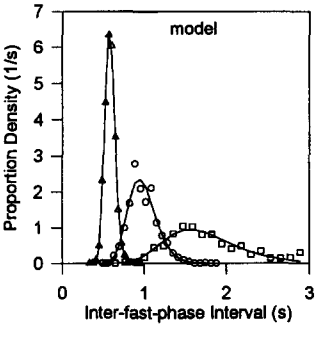

Fig. 7. Fitting the inverse Gaussian probability density function (pdf) to simulated inter-fast-phase intervals (IFPIs). The proportion density distributions of the IFPIs generated using the neural, integrate-to-fire model (Fig. 5) were determined for constant inputs of 0.25, 0.50 and 1.00 (*squares*, *circles* and *triangles*, respectively). Gaussian noise had mean 0 and variance 0.50 in all cases. A sample of the simulation at the input magnitude of 0.50 is shown in Fig. 6. The IFPI proportion density distributions were fit with the inverse Gaussian pdf (curves). The best fit parameters are given in Table 2

Table 2. Parameters for simulated inter-fast-phase interval (IFPI) proportion density distributions and for fits to the distributions of the inverse Gaussian probability density function (1)

Input	Drift rate (σ units)	Threshold (σ units)	Probability error	Bin width (s)	No. of bins	No. of intervals
0.25	2.907	5.035	0.025	0.118	25	564
0.50	5.690	5.620	0.028	0.066	45	1008
1.00	12.297	7.181	0.011	0.039	77	1706

Data were obtained by running the model diagrammed in Fig. 5. Details as per Table 1

4 Discussion

In the computational model presented above, which is based on neurophysiological observations, an element representing a population of vestibular nucleus neurons (VN in Fig. 5) integrates random noise as well as its constant input from the optokinetic system, and its output approximates a random walk with drift. This output is received by an element representing burst neurons (BN in Fig. 5) which fires a burst after its input from VN exceeds a threshold. The burst, which represents a fast-phase command, resets VN and the process is repeated. That process is analogous to a random walk with drift toward a threshold, where the probability density of the first threshold crossing times is described by the inverse Gaussian pdf (Seshadri 1993). This theoretical pdf (1) describes well the distributions of intervals between the fast phases of optokinetic nystagmus, at various constant levels of nystagmus, that were either simulated using the computational model, or determined experimentally in two different species (goldfish and turtle). The concordance of the theory with both the experimental and computational results supports the idea that fast-phase generation during constant velocity optokinetic nystagmus is analogous to a random walk with drift toward a threshold.

In that it takes the form of an integrate-to-fire mechanism, the model proposed here for optokinetic nystagmus resembles previous models of vestibular nystagmus (Schmid and Lardini 1976; Chun and Robinson 1978; Galiana 1991). As in the present model, the vestibular nystagmus models incorporated burst generators that fired a burst after they were brought to threshold by a signal related to eye position. However, the present optokinetic model differs in critical ways from those for vestibular nystagmus. The vestibular nystagmus models were either noise free (Schmid and Lardini 1976; Galiana 1991), or had noise introduced at the threshold stage (Chun and Robinson 1978). The burst elements in the vestibular nystagmus models were therefore not brought to threshold by anything resembling a random walk with drift, yet such a random walk is an essential feature of the present model of optokinetic nystagmus.

Another difference between the vestibular nystagmus models and the present model of optokinetic nystagmus involves the manner in which the burst itself is generated. In the vestibular nystagmus models, burst onset and offset are controlled by switches, and burst shape is controlled, at least in part, by black-boxes. In contrast, the present model for optokinetic nystagmus is a neural network in which threshold and burst shape are consequences only of the connections of the burst neuron (BN) with other neural elements that include those representing vestibular and pause neurons (VN and PN). The burst is generated by positive feedback of BN onto itself both directly and through PN. Neuroanatomical evidence indicates that excitatory burst neurons may exert positive feedback onto themselves through relays in the reticular formation (Strassman et al. 1986a, b). With BN exerting positive feedback on itself and receiving inhibition through the bias element (BS in Fig. 5), the loop through PN might appear to be superfluous. In fact, the integrate-to-fire behavior of the model is not dependent upon PN. However, including PN sharpens and greatly intensifies the BN bursts. A quantitative analysis of burst generation in this model will be described in a subsequent article.

The model can provide insight into fast-phase timing. The rate of fast-phase generation in the model is related to the rate at which BN reaches its threshold. This rate is set in part by the magnitude of the optokinetic input (IN in Fig. 5), and by the sensitivity of VN to it, which also determines the magnitude of the optokinetic response. By making the assumption that VN both drives the optokinetic slow phase and brings BN to threshold, the model can account for the finding that IFPIs decrease (and fast-phase rate increases) as optokinetic response magnitude increases (Fig. 3). The rate at which BN reaches threshold is also set by the weight of the connection to it from VN. This presumably varies among species and among individuals in a species, and can account for the finding that fast-phase rates can differ between individuals even if the magnitudes of their optokinetic responses are similar. It is also possible that the connection from VN to BN saturates at levels of optokinetic stimulation lower than those that saturate the optokinetic response. This could explain why drift rate estimates increase at a slower rate than goldfish optokinetic response magnitude as surround rotational velocity increases (Table 1A and B).

The most critical observation from the data is that, as optokinetic response magnitude decreases, the IFPI distribution broadens and intervals that are long relative to the mode become more common. This observation was made by Balaban and Ariel (1992) in the turtle. They suggested a timing model to explain the data, in which the next interval is a random proportion either of the previous interval or of a basic interval, and that long intervals occur when, under certain circumstances, the interval timing mechanism skips a cycle. The model

proposed here, which involves a random walk with drift toward a threshold, offers an alternative in which long intervals emerge naturally. The reason is that, as drift velocity decreases, it becomes more likely that any random walk can meander for a long time before it crosses the threshold. In the fast-phase model of Fig. 5, where the input to the burst generator approximates a random walk with drift and drift rate is analogous to optokinetic response magnitude, long IFPIs automatically become more common as optokinetic response magnitude decreases.

Acknowledgements. The author wishes to thank Dr. Peter Jung for suggesting the random walk analogy, and Dr. Ehtibar Dzhafarov for mathematical consultation. He would also like to thank Drs. Dzhafarov and Thomas Haslwanter for reading the manuscript, and Moses Keng for technical support. All procedures involving goldfish have been approved by the University of Illinois Laboratory Animal Care Advisory Committee under protocol number S2R317. This work was supported by National Science Foundation grant IBN 92-21823.

References

Allum JHJ, Graf W, Dichgans J, Schmidt CL (1976) Visual-vestibular interactions in the vestibular nuclei of the goldfish. Exp Brain Res 26:463–485

Balaban CD, Ariel M (1992) A 'beat-to-beat' interval generator for optokinetic nystagmus. Biol Cybern 66:203–216

Boyle R, Büttner U, Markert G (1985) Vestibular nuclei activity and eye movements in the alert monkey during sinusoidal optokinetic stimulation. Exp Brain Res 57:362–369

Cannon SC, Robinson DA, Shamma S (1983) A proposed neural network for the integrator of the oculomotor system. Biol Cybern 49:127–136

Chun K-S, Robinson DA (1978) A model of quick phase generation in the vestibuloocular reflex. Biol Cybern 28:209–221

Collewijn H (1975) Direction-selective units in the rabbit's nucleus of the optic tract. Brain Res 100:489–508

Curthoys IS, Nakao S, Markham CH (1981) Cat medial pontine reticular neurons related to vestibular nystagmus: firing pattern, location and projection. Brain Res 222:75–94

Easter SS (1972) Pursuit eye movements in goldfish (*Carassius auratus*). Vision Res 12:673–688

Galiana HL (1991) A nystagmus strategy to linearize the vestibulo-ocular reflex. IEEE Trans Biomed Eng 38:532–543

Galiana HL, Outerbridge JS (1984) A bilateral model for central neutral pathways in vestibuloocular reflex. J Neurophysiol 51:210–241

Hikosaka O, Maeda M, Nakao S, Shimazu H, Shinoda Y (1977) Presynaptic impulses in the abducens nucleus and their relation to postsynaptic potentials in motoneurons during vestibular nystagmus. Exp Brain Res 27:355–376

Hikosaka O, Igusa Y, Imai H (1978) Firing pattern of prepositus hypoglossi and adjacent reticular neurons related to vestibular nystagmus in the cat. Brain Res 144:395–403

Hoffmann K-P, Distler C (1989) Quantitative analysis of visual receptive fields of neurons in the nucleus of the optic tract and the dorsal terminal nucleus of the accessory optic tract in macaque monkeys. J Neurophysiol 62:416–428

Hoffmann K-P, Schoppmann A (1981) A quantitative analysis of the direction-specific response of neurons in the cat's nucleus of the optic tract. Exp Brain Res 42:146–157

Keller EL (1974) Participation of medial pontine reticular formation in eye movement generation in monkey. J Neurophysiol 37:316–332

Langer TP, Kaneko CRS (1984) Brainstem afferents to the omnipause region in the cat: a horseradish peroxidase study. J Comp Neurol 230:444–458

McCrea RA, Strassman A, May E, Highstein SM (1987) Anatomical and physiological characteristics of vastibular neurons mediating the horizontal vestibulo-ocular reflex of the squirrel monkey. J Comp Neurol 264:547–570

Nakao S, Curthoys IS, Markham CH (1980) Direct inhibitory projection of pause neurons to nystagmus-related pontomedullary reticular burst neurons in the cat. Exp Brain Res 40:283–293

Nakao S, Sasaki S, Schor RH, Shimazu H (1982) Functional organization of premotor neurons in the cat medial vestibular nucleus related to slow and fast phases of nystagmus. Exp Brain Res 45:371–385

Ohki Y, Shimazu H, Suzuki I (1988) Excitatory input to burst neurons from the labyrinth and its mediating pathway in the cat: location and functional characteristics of burster-driving neurons. Exp Brain Res 72:457–472

Remmel RS (1984) An inexpensive eye movement monitor using the scleral search coil technique. IEEE Trans Biomed Eng 31: 388–390

Robinson DA (1963) A method of measuring eye movement using a scleral search coil in a magnetic field. IEEE Trans Biomed Electron 10:137–145

Robinson DA (1975) Oculomotor control signals. In: Bach-y-Rita P, Lennerstrand G (eds) Basic mechanisms of ocular motility and their clinical implications. Pergamon Press, Oxford, pp 337–374

Robinson DA (1989) Control of eye movements. In: Brooks VB (ed) Handbook of physiology, sect 1: The nervous system, vol II, part 2. American Physiological Society, Bethesda, pp 1275–1320

Sasaki S, Shimazu H (1981) Reticulo-vestibular organization participating in generation of horizontal fast eye movement. Ann NY Acad Sci 374:130–143

Schmid R, Lardini F (1976) On the predominance of anti-compensatory eye movements in vestibular nystagmus. Biol Cybern 23:135–148

Seshadri V (1993) The inverse Gaussian distribution: a case study in exponential families. Clarendon Press, Oxford

Shimazu H (1983) Neuronal organization of the premotor system controlling horizontal conjugate eye movements and vestibular nystagmus. In: Desmedt JE (ed) Motor control mechanisms in health and disease. Raven Press, New York, pp 565–588

Shimazu H, Precht W (1966) Inhibition of central vestibular neurons from the contralateral labyrinth and its mediating pathway. J Neurophysiol 29:467–492

Strassman A, Highstein SM, McCrea RA (1986a) Anatomy and physiology of saccadic burst neurons in the alert squirrel monkey. I. Excitatory burst neurons. J Comp Neurol 249:337–357

Strassman A, Highstein SM, McCrea RA (1986b) Anatomy and physiology of saccadic burst neurons in the alert squirrel monkey. II. Inhibitory burst neurons. J Comp Neurol 249:358–380

Waespe W, Henn V (1977) Neuronal activity in the vestibular nuclei of the alert monkey during vestibular and optokinetic stimulation. Exp Brain Res 27:523–538

Watanabe S, Kato I, Sato S, Norita M (1993) Direct projection from the nucleus of the optic tract to the medial vestibular nucleus in the cat. Neurosci Res 17:325–329